

# Magnetospheric application of high-altitude long-duration balloon technology: Daylight auroral observations

X.-Y. Zhou <sup>a,\*</sup>, D. Lummerzheim <sup>b</sup>, G.R. Gladstone <sup>c</sup>, S.D. Gunapala <sup>a</sup>,  
S.B. Bandara <sup>a</sup>, J. Trihne <sup>a</sup>, L. Herrell <sup>a</sup>

<sup>a</sup> Jet Propulsion Laboratory, 4800 Oak Grove Drive, Pasadena, CA 91109, USA

<sup>b</sup> University of Alaska, 903 Koyukuk Drive, Fairbanks, AK 99775, USA

<sup>c</sup> Southwest Research Institute, 6220 Culebra Road, San Antonio, TX 78228, USA

Received 31 October 2006; received in revised form 25 January 2007; accepted 12 February 2007

## Abstract

Daylight auroral imaging is a proposed application of the NASA high-altitude long-duration balloon technology. This paper discusses the theoretical background of this application and test observations, for proof of the feasibility. It is demonstrated that nitrogen auroral emissions in the near-infrared band are detectable at altitudes of 35–40 km and above using a near-infrared InGaAs camera. The purpose of such observations is to identify auroral small-scale structures that are manifestations of auroral particle accelerations and the solar wind – magnetosphere – ionosphere interaction. Use of this new approach will enable studies of the dayside aurora, low-latitude aurora, and storm-time and substorm-time auroral conjugacy.

© 2007 COSPAR. Published by Elsevier Ltd. All rights reserved.

**Keywords:** Aurora; Auroral observations; Balloon technology; Magnetospheric application

## 1. Introduction

Application of scientific ballooning to magnetospheric and ionospheric studies began in the 1960s. These are mainly observations of auroral X-rays (Anderson, 1960; Anderson and Enemark, 1960; Brown, 1961; Smith et al., 1995; Millan et al., 2002) and high altitude electric fields (Holzworth, 1991; Curto et al., 2001). Optical auroral observations from balloons have not been carried out due to the overwhelming sunlight at visible wavelengths and due to the ozone absorption at ultraviolet wavelengths. This paper discusses a new approach of observing auroras at near-infrared (NIR) wavelengths from balloon altitudes. The significance of such observations for auroral science will be discussed as well.

Auroral morphology may give some indications of the auroral particle acceleration and source mechanisms in the magnetosphere. A diffuse aurora that lacks structure is typically produced by pitch angle scattered electrons that have a highly isotropic pitch angle distribution due to wave-particle interaction in the magnetosphere. Since the wave-particle interaction takes place without spatial structure, its ionospheric manifestation is accordingly a structureless diffuse aurora. For example, the interaction of an interplanetary fast forward shock with the magnetosphere can lead to whistler-mode instability. This, in turn, can isotropize the electron distribution and cause a diffuse aurora (Zhou and Tsurutani, 1999; Zhou et al., 2003). Discrete auroral forms, which exhibit small-scale dynamic structures on the other hand, are due to local acceleration mechanisms, such as the tearing mode instability above the ionosphere (Zhu et al., 2001; Otto and Zhu, 2003) or kinetic Alfvén waves (Chaston et al., 2003, 2005; Swift, 2004; Lysak and Song, 2005). The small-scale structures of discrete auroras are varied. Some discrete arcs are

\* Corresponding author.

E-mail address: [xiaoyan.zhou@jpl.nasa.gov](mailto:xiaoyan.zhou@jpl.nasa.gov) (X.-Y. Zhou).

mainly oriented in the west–east direction with large spatial scale (up to a thousand kilometers) and are relatively stable in shape and location, such as the arcs produced during substorm growth phases. Other arcs are very dynamic and abruptly change shape and location, such as the arcs produced during substorm expansion phases.

While the auroral small-scale structure is very important, it has often been a trade-off with the global auroral dynamics in space observations. A typical example is the interplanetary shock and/or solar wind pressure pulse generated aurora discovered by space-based remote sensing. Such an aurora was first reported based on the DE-1 UV images (with  $\sim 12$  min time resolution), which showed that the entire auroral oval lit up after a shock arrived at the Earth (Craven et al., 1986). With a higher temporal resolution ( $\sim 37$  s), the Polar UVI data showed that the aurora occurred not only at local noon right after the shock impingement (within 37 s), but also propagated anti-sunward at a very high speed along the auroral oval (Spann et al., 1998; Zhou and Tsurutani, 1999; Brittnacher et al., 2000; Vorobjev et al., 2001; Boudouridis et al., 2003, 2004). Later it was found that the auroral onset near local noon expanded to lower magnetic latitudes as well. The low latitude aurora occurred mainly in the noon sector of 10–14 MLT, sometimes in patches connected to or disconnected from the main oval (Liou et al., 2002) and sometimes occurring as a proton auroral spot at mid  $50^\circ$  MLat (Zhang et al., 2002; Hubert et al., 2003). Although the Polar UVI images offer higher temporal and spatial resolution than the DE-1 images, it is very difficult to resolve small-scale auroral structures in UVI images. Diffuse and discrete auroral structures cannot be distinguished, nor, therefore, can particle acceleration mechanisms.

Particle and wave observations from the FAST and DMSP spacecraft showed that during shock-auroras, highly structured field-aligned currents are generated at the poleward boundary of the auroral oval. Precipitating electrons in the currents are soft electrons with energies lower than  $\sim 1$  keV and with pitch angles peaking at  $0^\circ$  and  $180^\circ$ . Broadband waves are also observed in the currents where the soft electrons have large  $V_{\parallel}$  in both directions parallel and anti-parallel to the magnetic field. This signature indicated that these electrons are very likely accelerated by kinetic Alfvén waves. At lower latitudes along the oval, electrons have higher energy ( $> 1$  keV) and are highly isotropic. These latter electrons are pitch angle scattered due to adiabatic compression (Zhou et al., 2003). For the mid-day low latitude auroral patches in the Polar UVI images, the DMSP data show that the precipitating electrons have energies at 5–10 keV and precipitating ions are at lower energies of 0.1–1 keV (Liou et al., 2002). The electron energy level is consistent with the speculation of adiabatic compression. For the intense detached proton auroras in the IMAGE SI-12 images, the ions reached  $\sim 10$  keV in the DMSP observations (Zhang et al., 2002). Since the DMSP SSJ instrument only sees par-

ticles in the loss cone, its data have not provided enough information to eliminate specific electron and proton acceleration of the mid-day low latitude aurora. In general, spatial and temporal variation of auroral small-scale structures cannot be distinguished using satellite in situ particle and wave measurements. This hampers the interpretation of observations of shock-induced auroras.

In contrast, imaging observations from the ground provide spatial and temporal variations at high resolution. Ground-based imaging can provide detailed information about auroral small-scale structures. However, to conduct daylight auroral imaging from the ground is impractical, due to sunlight contamination and limited land area at auroral latitudes. Although there are some observatories in Antarctica and the Arctic conducting dayside auroral imaging observations during local winter, the moon light and cloudy weather makes the limited observation opportunity even less. Dayside auroras generated by shocks and pressure pulses take place in the oval and at low latitudes to  $\sim 55^\circ$  MLat. At this latitude the sky is too bright, even in winter, to conduct daytime auroral imaging from the ground. Therefore, we have proposed to go to higher altitudes and longer wavelengths, where the auroral signal over background (AoB) ratio is high enough to allow auroral imaging (Zhou et al., 2007). This idea was inspired by theory and model predictions of decreasing sunlit sky brightness toward longer wavelengths and higher altitudes as well as the development of the NASA high-altitude long-duration balloon technology.

In the following sections, we will discuss the sky brightness variation with wavelength and altitude, results of an auroral test observation from Poker Flat, and applications of this new approach. Our study confirmed that the aurora can be detected at balloon altitudes of 35–40 km and above. Applications of the balloon-based auroral observations using near-infrared (NIR) cameras include dayside and conjugate auroral observations.

## 2. Sky brightness

A key parameter that decides whether an aurora can be seen is the AoB ratio. For a visible wavelength camera, an aurora is identifiable when the AoB ratio is larger than approximately 0.1. To have a large AoB ratio, one needs either a very bright aurora or dark sky. To understand the sky brightness variation, we have utilized an atmospheric radiance model, the MODTRAN (MODerate spectral resolution atmospheric TRANsmittance algorithm and computer) model (Anderson et al., 1999). It was developed by AFRL/VSBT in collaboration with Spectral Sciences, Inc. The model calculates atmospheric transmittance and radiance for wavenumbers from 0 to  $50,000 \text{ cm}^{-1}$  at moderate spectral resolution, primarily  $2 \text{ cm}^{-1}$  ( $20 \text{ cm}^{-1}$  in the UV). Except for its molecular band model parameterization, the MODTRAN model has capabilities including spherical refractive geometry, solar and lunar source func-

tions, and scattering (Rayleigh, Mie, single, and multiple), and default profiles (gases, aerosols, clouds, fog, and rain).

The sky brightness calculated using the MODTRAN model in the wavelengths from 200 to 2000 nm is shown in Fig. 1, in which the local zenith angle (LZA) is 60°, and the local azimuth (LAZ) is 90°. Fig. 1a shows the sky brightness from 30 to 50 km altitude for a solar zenith angle (SZA) of 55°. This SZA roughly corresponds to the maximum solar elevation during local summer in Antarctica or the Arctic. It is very obvious that the brightness decreases when the wavelength or altitude increases. From 30 to 50 km, the brightness reduces by more than an order of magnitude for all wavelengths longer than ~300 nm. The model shows that in the wavelengths between 1000 and 1600 nm, which is indicated by the box in Fig. 1a, the brightness is basically below 100 kR/nm at an altitude of 35 km and above. There are bright auroral emissions in this wavelength range, such as the N<sub>2</sub><sup>+</sup> Meinel bands at 1109 nm and N<sub>2</sub> 1st positive bands at 1236 nm. The two vertical lines indicate these two wavelengths. Fig. 1b shows the sky brightness from the ground to 50 km when SZA = 96°. This solar zenith angle indicates the sun is 6° below the horizon, in the limit of civil twilight (i.e., during 0°–6° depression angle). The sky brightness at the ground level (the black dotted line) provides a reference for the auroral test observation that will be discussed in the next section. The dips at z = 0 km altitude sky brightness curve are due to tropospheric absorption at these wavelengths.

Comparing auroral brightness with the sky brightness at 40 and 50 km altitudes in Fig. 1a, the AoB ratios of N<sub>2</sub><sup>+</sup> Meinel and N<sub>2</sub> 1st positive emissions are calculated for an ICB3 aurora (Vallance Jones, 1974) and shown in Fig. 2. At each emission, the top symbol gives the AoB ratio at the 50 km and the bottom gives the ratio at

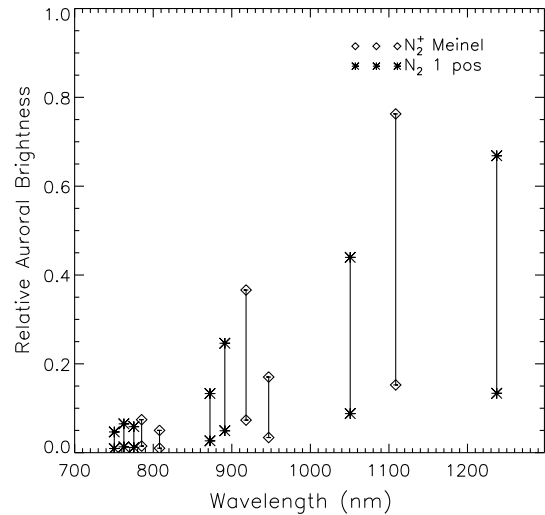


Fig. 2. Auroral signal over background (AoB) ratio of nitrogen emissions. The top symbols of each emission are for 50 km altitude and the bottom symbols are for 40 km.

40 km altitude. The figure shows that the AoB ratio enhances towards longer wavelengths. It is mainly because the background brightness decreases towards longer wavelengths as shown in Fig. 1. At 1109 and 1236 nm, the AoB ratios are greater than ~0.1 at 40 km and are greater than ~0.7 at the 50 km altitude. This result suggests that near-infrared nitrogen emissions are detectable using an imaging instrument at 40 km altitude or above. Such a platform is available with a high-altitude balloon. A candidate instrument is a NIR InGaAs camera that has the best quantum efficiency (more than 50%) between 1000 and 1600 nm. A more description of the InGaAs detector and the camera can be found in Zhou et al. (2007).

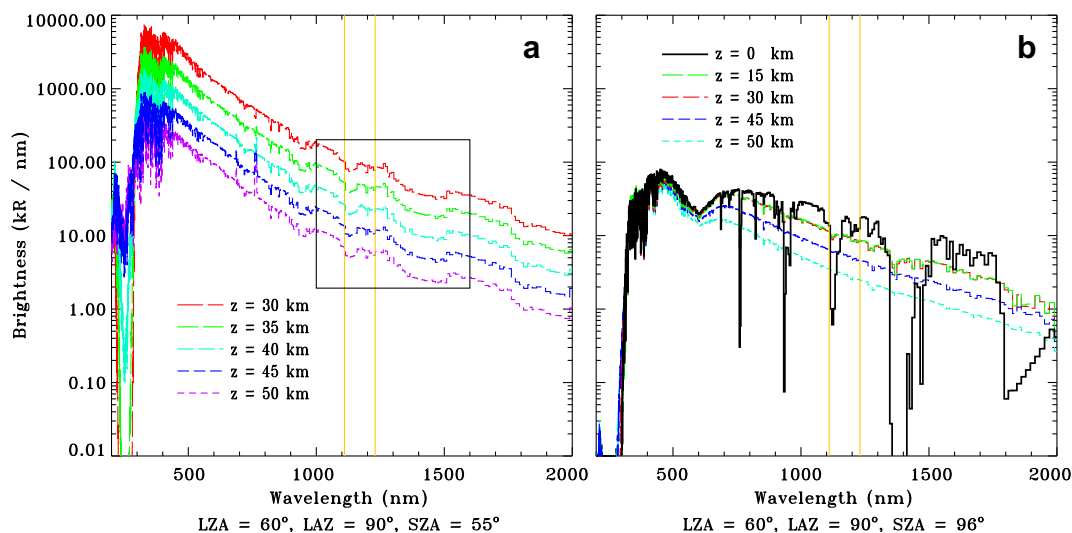


Fig. 1. MODTRAN model radiance for sky brightness from 200 to 2000 nm. The two auroral emission wavelengths at the vertical lines are 1109 and 1236 nm. (a) The sky brightness when the sun is at the highest elevation in local summer at the poles. (b) The sky brightness when the sun is 6° below the horizon. Dips in the black dotted line at z = 0 km altitude are due to tropospheric absorption.

### 3. Auroral imaging in twilight

Encouraged by the results shown in Figs. 1 and 2, we conducted test observations from the ground at the Poker Flat Research Range (65N, 147W) using a NIR InGaAs camera in March and April 2005. The camera has a  $9^\circ$  solid cone field-of-view and was pointed north about  $30^\circ$  above the horizon. For comparison, a consumer Nikon D-100 6 megapixel color camera was pointed in the same direction with a similar field of view. The NIR camera had a cadence and exposure time of 1 s and the Nikon was set up with a cadence of 1 min and 10 s exposures. The observations were conducted during twilight and night from March 22 to April 26, 2005. The purpose of the test observations was to demonstrate auroral imaging during twilight, when the sky has a brightness of about 50–100 kR/nm, and to investigate the NIR camera performance at different sky brightness levels. Fig. 3 shows the auroral images obtained on April 13 near 0617 UT, which corresponds to 2117 LT and a SZA at  $96^\circ$  at Poker Flat. Images from left to right are the raw NIR image, the same NIR image after the background was removed, and the Nikon image at 0617 UT. In the raw image, the aurora is barely seen due to a very bright background that includes not only twilight but also a contribution of OH airglow. In the middle image, auroral fine structures are prominent after subtracting an estimated background. The aurora quickly moved across the camera field-of-view within 10 s (see more auroral images in Zhou et al., 2007). The determination of the estimated background is discussed in more detail later on. The Nikon image does not show the aurora in part because of the long exposure time, and in part because of the bright twilight background.

Around 0600 UT on April 13 there was some minor geomagnetic activity with AL at about  $-300$  nT and  $D_{st}$  at  $-53$  nT. This level of geomagnetic activity continued all night, and we observed some auroral activity in darkness. Focusing on the aurora in twilight, Fig. 4 shows a summary of about one hour of observations when the sky gradually became dark from 2110 to 2215 LT. The bottom panel of Fig. 4 shows the average brightness of each image at every second. From about 0645 UT (i.e., 2145 LT at Poker Flat) onward, the average sky brightness was

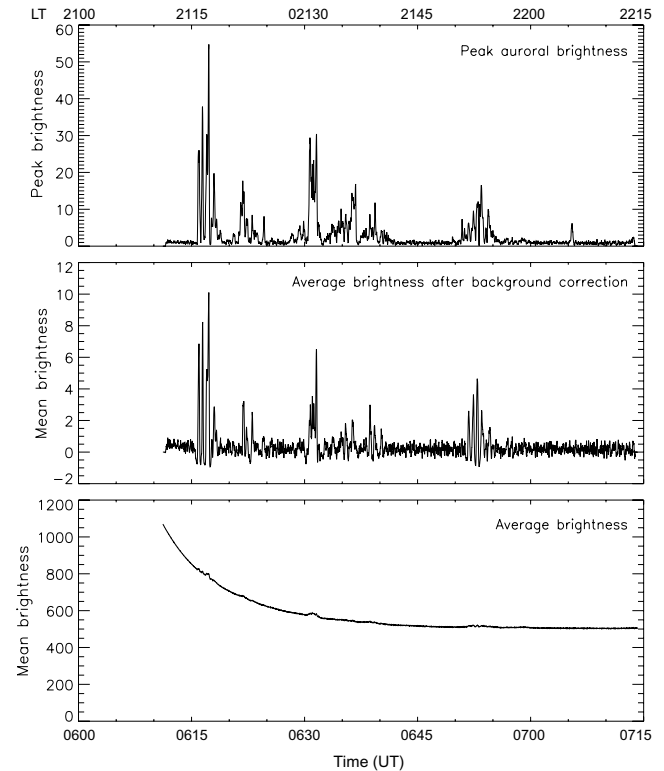


Fig. 4. Overview of average and peak image brightness from 0610 to 0715 UT April 13, 2005. The corresponding local time (LT) is shown on the top.

$\sim 500$  counts. This brightness is mainly attributed to the airglow of OH3-1, OH4-2 and OH5-3 in 1430–1700 nm (Oliva and Origlia, 1992; Remick et al., 2001). To accentuate the small increases seen in the average image brightness near 0616, 0631, and 0653 UT, which are due to the presence of the aurora in parts of the images, the middle and top panels show the image brightness after the background removal. The middle panel is the average brightness of each image. Since the aurora occupied only part of the image we also plotted the peak brightness that is shown in the top panel. The peak auroral brightness above the background is 37 counts for the aurora at 0616:30 UT. Both top and middle panels show that after the background removal the residual noise is a very low level and not more than 3 counts. This figure indicates that we can distinguish an

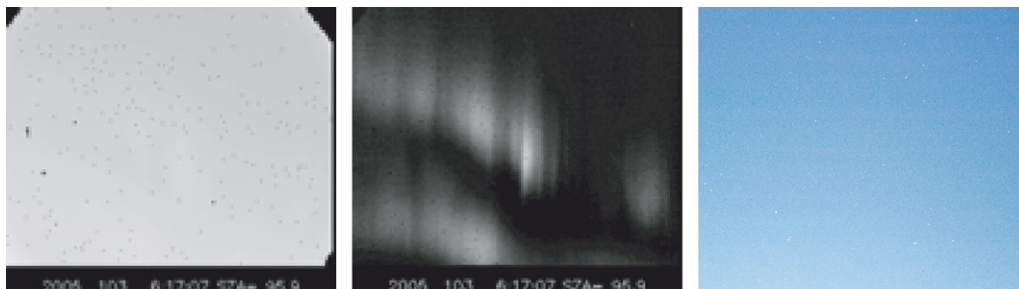


Fig. 3. Auroral test observation from Poker Flat under twilight at 0617:07 UT April 13, 2005. From left to right are the raw image from the NIR camera, the NIR image after the background removal, and the Nikon image.

aurora at very low AoB ratios, which are less than 0.063 at 0616 UT and less than 0.05 at 0630 UT. The InGaAs camera has a 12 bit detector (i.e., the dynamic range is 4096 counts). In the absence of any noise, the camera is capable to identify a signal even at only 1 count (i.e., a signal over background ratio at  $\sim 0.00025$ ). The example in Fig. 4 shows that the background estimation is sufficiently reliable to identify aurora that is only 10 counts above that background. For a nearly saturated image this would translate to an AoB ratio requirement of only 0.0025 for this InGaAs camera.

Since the OH airglow brightness did not change much with the solar zenith angle during the observation time, the bottom panel of Fig. 4 indicates that the twilight brightness is  $\sim 300$  counts at  $\sim 0617$  UT. The MODTRAN radiance does not include the OH airglow contribution. Therefore, the aurora shown in Fig. 3 was actually detected in a brighter sky than the brightness shown by the dot line in Fig. 1b. The actual background brightness is  $\sim 2.7$  times brighter than the model prediction, which is shown by a black solid curve in Fig. 5. This figure shows the comparison of the brightest sky at the pole local summer and the sky when the aurora was detected. The comparison indicates that the auroral background in Fig. 3 corresponds to the sky brightness between 35 and 40 km altitudes. It should be noted that 35 km is a routine altitude of NASA scientific balloons. NASA has demonstrated a new balloon technology and has flown a balloon up to 50 km altitude with 700 kg payload for about 20 h (see NASA press release at <http://www.gsfc.nasa.gov/news-release/releases/2002/h02-163.htm>). It should be also noted that a full developed NIR camera for balloon-based observations will include a narrow bandpass filter to restrain the most

intense OH airglow in 1430–1700 nm that is  $\sim 8$  times brighter than the near-infrared nitrogen emissions (Remick et al., 2001). Therefore, it is reasonable to apply a factor of 2.7 to estimate the background brightness at  $\sim 0617$  UT and to compare with the MODTRAN radiance at 30–50 km altitude.

The sky background was estimated from the observed sky brightness over time. One could calculate a long term fit to the brightness of each image pixel as a function of local solar zenith angle by examining many days of data. This fit could serve to estimate the combined twilight and airglow background. In order to avoid excessive computer time, and to smooth out the background we did a similar calculation for each row of pixels of the images. Since the small field-of-view and the viewing geometry toward the northern sky, the sky brightness should only be a function of elevation, i.e., the row number in the image. The auroral episodes in any give part of the image were brief during the night of April 13. Rather than fitting several nights of image brightness to solar zenith angle, we limited the analysis to fitting a smooth function to the average brightness of each image row over the one-hour period presented in Fig. 4. By using a low order Legendre polynomial representation for the fit, the auroral brightness is reduced much less after the background removal than using simple average. This fit is then assumed to represent the sky brightness in the absence of aurora for any given time and image row. A complete background image can be constructed from the averaged row brightness and can be subtracted from the original image.

#### 4. Potential applications

We have addressed two key questions for auroral observations in sunlight, i.e., whether the AoB ratio is high enough at balloon altitudes so that the aurora can be detected, and what is a proper instrument technology that can distinguish the aurora from the sky background at a 0.1 (or lower) AoB ratio. It is demonstrated that the near infrared nitrogen auroral emissions are detectable in sunlight at balloon altitudes of 35–40 km and above using a NIR InGaAs camera.

There are some major applications of this new approach to space physics studies. First are the dayside and lower latitude dayside auroral observations. As we have discussed in the introduction section, dayside aurora can take place at very low latitude during an intense magnetospheric compression, such as  $\sim 55^\circ$  MLat. At these low latitudes the sunlight is too bright to do high resolution auroral imaging from the ground even during local winter. Using this new approach, speculations about the dayside auroral generation (such as in Spann et al., 1998; Liou et al., 2002; Zhou et al., 2003; Zhang et al., 2002; Zhou et al., in press) can be examined by observing auroral small-scale structure to distinguish diffuse and discrete auroral arcs.

In addition to dayside auroral observations, another significant science application is conjugate auroral

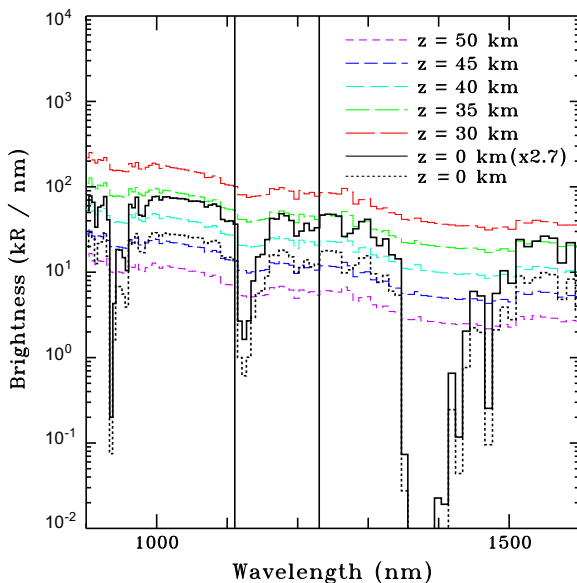


Fig. 5. Comparison of sky brightness at 30, 35, 40, 45, and 50 km altitudes with  $\text{SZA} = 60^\circ$ . The black dotted line is the twilight brightness at the ground at 0617 UT. The black solid curve is corrected sky brightness at the ground at 0617 UT when the aurora was observed as shown in Fig. 3. The two vertical lines are the same wavelengths as in Fig. 1.

observations. Such observations have important implications for substorm studies. The onset of a substorm expansion phase occurs in the equatorial magnetotail, which should have significant manifestation in the nightside auroral ionosphere in both the northern and southern hemispheres. Some recent studies have shown that poleward auroral surges during substorm expansion phases may not be conjugate (Frey et al., 1999; Mende et al., 1999), which led to some important questions related to our current understanding of substorm dynamics and auroral particle accelerations. Auroral conjugacy can be used as a large-scale visible diagnostic for processes in the invisible magnetosphere (Stenbaek-Nielsen and Otto, 1997). Conjugate auroral observations can be achieved when balloon measurements in the Antarctic summer are simultaneously conducted with winter observations in the northern hemisphere using existing ground-based all-sky imager arrays, such as the IMAGE, DMI, THEMIS, and Alaskan arrays. It should be mentioned that the lack of studies of auroral substorms in the southern hemisphere is mainly due to the fact that the nightside aurora oval is above the ocean in most of the time. Therefore, observations from the ground are very rare.

Another interesting study using this new method would be the extremely high altitude aurora (Mizuno et al., 2005). The aurora detected by the Solar Mass Ejection Imager (SMEI) was possibly extended to visible altitudes of 2000 km or higher. The SMEI on the Coriolis satellite is a sensitive scanning instrument that assembles an approximate all-sky image of the heliosphere in red-biased visible light once per orbit. Whether the “SMEI aurora” is auroral emission or resonance scattering, the observation from the NIR InGaAs camera will provide an answer, for the NIR camera only can detect the former but not the latter.

## 5. Conclusion and further comments

Auroral observations in sunlight can reveal dayside auroral small-scale structure and can help to identify auroral particle acceleration mechanisms and characteristics of auroral conjugacy during storms and substorms. Our studies have confirmed that auroral observations using a NIR camera onboard balloons is feasible. The technique is relatively simple, easy to apply, and is very cost effective in comparison with satellite missions.

Although the aurora in twilight has been observed by this JPL-built InGaAs camera, improvements are necessary for future balloon-based observations. The new NIR camera system should include an InGaAs detector, a NIR all-sky optical system, a bandpass filter, and an electronic and software package. The detector will have a  $640 \times 512$  (or larger) focal plane array with pixel size of  $25 \times 25 \mu\text{m}$ , which can resolve auroral structures in the size of 0.3 at 50 km distance and 6.3 at 1000 km distance. The all-sky field-of-view will allow a flexibility of seeing auroras in all directions. The filter focuses at 1109 nm to exclude not only the scattered sunlight, but also the OH airglow.

The electronic and software package will provide the observation control, telemetry control first stage data processing, and data storage, etc. It should be noted that such a camera system has low mass ( $\sim 5$  kg) and low power consumption ( $\sim 5.5$  W) which are significant advantages for balloon flights. The camera is suitable for piggyback flights and/or to be flown alone.

## References

- Anderson, K.A. Balloon observations of X-rays in the auroral zoon, I. *J. Geophys. Res.* 65, 551–564, 1960.
- Anderson, K.A., Enemark, D.E. Balloon observations of X-rays in the auroral zoon, II. *J. Geophys. Res.* 65, 3521–3538, 1960.
- Anderson, G.P., Berk, A., Acharya, P.K., et al. MODTRAN4: radiative transfer modeling for remote sensing. *Proc. SPIE, Opt. Atmospheric Propagation Adaptive Syst. III* 3666, 2–10, 1999.
- Boudouridis, A., Zesta, E., Lyons, L.R., Anderson, P.C., Lummerzheim, D. The effect of solar wind pressure pulses on the size and strength of the auroral oval. *J. Geophys. Res.* 108, 8012–8027, doi:10.1029/2002JA009373, 2003.
- Boudouridis, A., Zesta, E., Lyons, L.R., Anderson, P.C., Lummerzheim, D. Magnetospheric reconnection driven by solar wind pressure fronts. *Ann. Geophys.* 22, 1367–1378, 2004.
- Brittnacher, M., Wilber, M., Fillingim, M., Chua, D., Parks, G., Spann, J., Germany, G. Global auroral response to a solar wind pressure pulse. *Adv. Space Res.* 25, 1377–1385, 2000.
- Brown, R.R. Balloon observations of auroral X-rays. *J. Geophys. Res.* 66, 1379–1387, 1961.
- Chaston, C.C., Bonnell, J.W., Carlson, C.W., McFadden, J.P., Strangeway, R.J., Ergun, R.E. Kinetic effects in the acceleration of auroral electrons in small scale Alfvén waves: a FAST case study. *Geophys. Res. Lett.* 30, doi:10.1029/2002GL015777, 2003.
- Chaston, C.C., Peticolas, L.M., Carlson, C.W., McFadden, J.P., Mozer, F., Wilber, M., Parks, G.K., Hull, A., Ergun, R.E., Strangeway, R.J., Andre, M., Khotyaintsev, Y., Goldstein, M.L., Acuña, M., Lund, E.J., Reme, H., Dandouras, I., Fazakerley, A.N., Balogh, A. Energy deposition by Alfvén waves into the dayside auroral oval: cluster and FAST observations. *J. Geophys. Res.* 110, doi:10.1029/2004JA010483, 2005.
- Craven, J.D., Frank, L.A., Russell, C.T., Smith, E.E., Lepping, R.P. Global auroral responses to magnetospheric compressions by shocks in the solar wind: two case studies, in: Kamide, Y., Slavin, J.A. (Eds.), *Solar Wind-Magnetosphere Coupling*. Terra Scientific, Tokyo, pp. 367–380, 1986.
- Curto, J.J., Alberca, L.F., Holzworth, R.H., de la Morena, B., et al. Electric conductivity and electric field in the stratosphere: middle-latitude balloon flight results. *J. Geophys. Res.* 106, 21337–21342, 2001.
- Frey, H.U., Mende, S.B., Vo, H.B., et al. Conjugate observation of optical aurora with Polar satellite and ground-based cameras. *Adv. Space Res.* 23, 1647–1652, 1999.
- Holzworth, R.H. Conductivity and electric field variations with altitude in the stratosphere. *J. Geophys. Res.* 96, 12857–12864, 1991.
- Hubert, B., Gerard, J.C., Fuselier, S.A., Mende, S.B. Observation of dayside subauroral proton flashes with the IMAGE-FUV imagers. *Geophys. Res. Lett.* 30, 1145–1148, doi:10.1029/2002GL016464, 2003.
- Liou, K., Wu, C.-C., Lepping, R.P., Newell, P.T., Meng, C.-I. Midday sub-auroral patches (MSPs) associated with interplanetary shocks. *Geophys. Res. Lett.* 29 (16), doi:10.1029/2001GL014182, 2002.
- Lysak, R.L., Song, Y. Nonlocal interactions between electrons and Alfvén waves on auroral field lines. *J. Geophys. Res.* 110, doi:10.1029/2004JA010803, 2005.
- Mende, S.B., Frey, H.U., Geller, S.P., et al. Multistation observations, of auroras: polar cap substorms. *J. Geophys. Res.* 104, 2333–2342, 1999.
- Millan, R.M., Lin, R.P., Smith, D.M., Lorentzen, K.R., McCarthy, M.P. X-ray observations of MeV electron precipitation with a balloon-borne germanium spectrometer. *Geophys. Res. Lett.* 29, 2194–2197, 2002.

- Mizuno, D.R., Buffington, A., Cooke, M.P., et al. Very high altitude aurora observations with the Solar Mass Ejection Imager. *J. Geophys. Res.* 110, doi:10.1029/2004JA010689, 2005.
- Oliva, E., Origlia, L. The OH airglow spectrum: a calibration source for infrared spectrometer. *Astron. Astrophys.* 254, 466–471, 1992.
- Otto, A., Zhu, H., in: Büchner, J., Dum, C., Scholer, M. (Eds.), *Fluid Plasma Simulation of Coupled Systems: Ionosphere and Magnetosphere*, Space Plasma Simulation, Lecture Notes in Physics, vol. 615. Springer, pp. 193–211, 2003.
- Remick, K.J., Smith, R.W., Lummerzheim, D. The significance of resonant scatter in the measurement of  $N_2^+$  first negative 0–1 emissions during auroral activity. *J. Atmo. Solar-Terr. Phys.* 64, 295–308, 2001.
- Smith, D.M., Lin, R.P., Anderson, K.A., Hurley, K., Johns, C.M. High-resolution spectra of 20–300 keV hard X-rays from electron precipitation over Antarctica. *J. Geophys. Res.* 100, 19675–19685, 1995.
- Spann, J.F., Brittacher, M., Elsen, R., Germany, G.A., Parks, G.K. Initial response and complex polar cap structures of the aurora in response to the January 10, 1997 magnetic cloud. *Geophys. Res. Lett.* 25, 2577–2580, 1998.
- Stenbaek-Nielsen, H.C., Otto, A. Conjugate auroras and the interplanetary magnetic field. *J. Geophys. Res.* 102, 2223–2232, doi:10.1029/96JA03563, 1997.
- Swift, D.W. Use of a hybrid code for global-scale simulation of the Earth's magnetosphere. *Comput. Phys. Comm.* 164, 370–376, doi:10.1016/j.cpc.2004.06.049, 2004.
- Vallance Jones, A. *Aurora*. Reidel Publishing, Dordrecht, Holland, 301 p, 1974.
- Vorobjev, V.G., Yagodkina, O.I., Sibeck, D.G., Liou, K., Meng, C.-I. Polar UVI observations of dayside auroral transient events. *J. Geophys. Res.* 106, 28897–28912, 2001.
- Zhang, Y., Paxton, L.J., Immel, T.J., Frey, H.U., Mende, S.B. Sudden solar wind dynamic pressure enhancements and dayside detached auroras: IMAGE and DMSP observations. *J. Geophys. Res.* 108, doi:10.1029/2002JA009355, 2002.
- Zhou, X.-Y., Tsurutani, B.T. Rapid intensification and propagation of the dayside aurora: large scale interplanetary pressure pulses (fast shocks). *Geophys. Res. Lett.* 26, 1097–1100, 1999.
- Zhou, X.-Y., Strangeway, R.J., Anderson, P.C., Tsurutani, B.T., Haerendel, G., Sibeck, D.G., Frey, H., Arballo, J.K. Shock-aurora: FAST and DMSP observations. *J. Geophys. Res.* 108 (A4), 8019–8035, doi:10.1029/2002JA009701, 2003.
- Zhou, X.-Y., Lummerzheim, D., Gladstone, R., Gunapala, S. Feasibility of observing dayside aurora using nir camera onboard high-altitude balloons. *Geophys. Res. Lett.* 34, L03105, doi:10.1029/2006GL028611, 2007.
- Zhou, X.-Y., Sibeck, D.G., Amm, O., Ruohoniemi, J.M. Interplanetary shock generated ionospheric traveling convection vortex near local noon, *Ann. Geophys.*, in press.
- Zhu, H., Otto, A., Lummerzheim, D., Rees, M.H., Lanchester, B.S. Ionosphere-magnetosphere simulation of small scale structure and dynamics. *J. Geophys. Res.* 106, 1795–1806, 2001.